Projected Increase in Hydrologic Extremes in the Mid-21st Century for Northeastern United States

Sujan Pal[1], Jiali Wang[1], Jeremy Feinstein[1], Eugene Yan[1], Veerabhadra Rao Kotamarthi[1]

[1]Environmental Science Division, Argonne National Laboratory, Lemont, IL, USA

Corresponding author: Sujan Pal (spal@anl.gov)

Key Points:

- Extreme river flows are projected to increase in winter months.
- Extreme inland flooding is projected to increase in intensity and spatial extent.
- Evapotranspiration and soil moisture increase while snowpack decreases in the future.

Abstract

Assessing the changes in future extreme hydrologic conditions due to climate change is essential. This study investigates the potential impacts of climate change on precipitation, streamflow and inland flooding in Northeast United States (NEUS) during the mid-21st century. Dynamically downscaled climate projections from global climate models were obtained using the Weather Research and Forecasting (WRF) model over the North American continent. These were used to drive a high-resolution hydrologic model WRF-Hydro over NEUS. We performed three 10-year long simulations for historical (1995-2004) and future (2045-2054) periods under business-as-usual scenarios at a spatial resolution of 200 meters. A general extreme value model was developed to project the risks associated with low-frequency events. Results from four major watersheds indicate a significantly wetter regime in peak winter months and potential drier conditions during late spring to early summer. Discharges in fall are projected to decrease in the northern watersheds and increase towards the south. Extreme flow, and water depths resulting from extreme inland flooding are projected to increase by 5-20% and >100%, respectively. Extent of the total flooded area is likely to be 20% greater by the mid-century. These increased risks can be attributed to: 1) approximately 25% increase in decadal mean, and >75% increase in decadal maximum precipitation intensity, 2) up to 30% lower snow availability and 5-25% higher evapotranspiration throughout the year, and 3) a projected 5% increase in soil moisture in all seasons except summer. Furthermore, rapid snow melting in winter might cause an earlier peak flow in the rivers.

Plain Language Summary

Climate change is expected to have significant impacts on the future hydrology of the Northeast United States (NEUS). Streamflow and inland flooding are expected to change in response to future changes in temperature and precipitation. This study applied a regional climate model to downscale historic and future climate information from three coarse-resolution global climate models. Next, a high-resolution inland hydrologic model was forced with those downscaled outputs to investigate critical changes in the streamflow rates, water pooling depths, soil moisture and evaporation rates. Decade long 'Future' simulations (2045-2054) were compared to the 'Historic' ones (1995-2004). We find that the changes in extreme precipitation are higher in magnitude than changes in mean precipitation. Mean river flow is projected to increase in winter and decrease in summer with the timing of peak flow shifting earlier in the spring. Models predict increases in extreme flow in four major rivers of NEUS – Connecticut, Delaware, Hudson, and Potomac. Moreover, extreme inland flooding intensity is projected to increase, affecting more regions of NEUS. Models predict the amount of snowpack to decrease, and evapotranspiration to increase due to a warmer climate in future. The findings are critical for water managers and stakeholders of NEUS in decision making.

1 Introduction

Earth's climate is changing primarily due to increasing amount of carbon dioxide (CO_2) and other greenhouse gases in the atmosphere. Observations indicate that human-induced global warming reached approximately 1^{o}C above pre-historic levels in 2017 and is likely to reach to 1.5^{o}C above pre-industrial levels by 2040 (Allen et al., 2018). Intergovernmental Panel on Climate Change (IPCC) suggested a global temperature rise between 2.0 to 4.2^{o}C by the end of 21st century (Pachauri et al., 2014). As Clausius-Clapeyron equation suggests about 7% increase in the moisture holding capacity of the atmosphere per degree of warming (Trenberth, 1999; Allan and Soden, 2008), climate change is expected to impact the future hydrologic cycle. This has important implications for flooding, water resources, and ecosystems. Multiple studies have projected potential changes in temperature (Dai, 2012; Karmalkar and Bradley, 2017), precipitation (Allen and Ingram, 2002; Groisman et al., 2005; Shaw et al., 2011; Pendergrass et al., 2017), tropical storms and hurricanes (Seneviratne et al., 2012), droughts and floods (Tebaldi et al., 2006), evaporation rates (Condon et al., 2020; Konapala et al., 2020), snow pack amounts (Fyfe et al., 2017), streamflow (Naz et al., 2016; Byun et al., 2019), sea level rise (Yin et al., 2009; Kulp and Strauss, 2019), surface energy budget (Hu et al., 2019) and water budget (Leta et al., 2016) due to climate change. These changes have cascading effects to existing infrastructures, freshwater ecosystem, aquatic habitats, droughts, hydropower, water quality and so on.

Northeastern United States (NEUS) has seen significant increases in extreme precipitation events in the past five decades (Melillo et al., 2014; Parr et al., 2015a; Walsh et al., 2014). It is identified to be highly vulnerable to climatic changes (Hayhoe et al., 2007; Wuebbles et al., 2017; Siddique et al., 2021). While the intensity of the most extreme precipitation events (or the heaviest 1% of all daily events) have increased in every region of the contiguous US since the 1950s, the maximum change in precipitation intensity of extreme events occurred in the NEUS reached 71% (Melillo et al. 2014). Moreover, changing rainfall characteristics are expected to influence the other components of the hydrologic cycle, including streamflow, soil moisture and evapotranspiration (ET), having direct impacts on droughts and floods (Horton et al., 2014; Bose et al., 2017). Several studies have investigated the potential future changes in some of these aspects, mostly at different sub-regions of NEUS. For example, increased occurrences of flooding, compared to historic flooding records, have been identified (Collins, 2009; Armstrong et al., 2014; Demaria et al., 2016a; Siddique et al., 2020). An increase in annual ET at the rate of around 3 cm per ^{o}C of temperature increase, with a consequent reduction of April-May runoff in New England, was documented in Huntington (2009). Marshall and Randhir (2008) suggested a 12-22% decrease in runoff in the Connecticut watershed depending on CO_2 emission scenarios. Due to the dependence of runoff on snowmelt, timings of discharges are also important in NEUS. Hayhoe et al. (2007), Berton et al. (2016), Villarini (2016), Dhakal and Palmer (2020) identified potential changes in the timings and seasonality of flood events. Hodgkins et al. (2003) and Kam et al. (2016) indicated higher winter discharges and earlier peak discharges in spring in a warmer climate. Additionally, Parr et al. (2015b) found an increase in soil moisture during winter and spring (due to precipitation increase) and decrease in autumn and summer (due to increase in ET, up to 0.2 mm/day) in the Connecticut watershed. While most of the above-mentioned studies looked at discrete watersheds, very few studies gave a region-wide analysis of future hydrological characteristics using detailed meteorological drivers developed from a high resolution dynamically downscaled dataset. Demaria et al. (2016b) investigated effects of climate change on streamflow and seasonal snowpack over a large region covering NEUS and Midwest. They found positive trends in 3-day peak flows and negative trends in 7-day low flows along with statistically significant decreases in snow water equivalent ([SWE], depth of water that would result from complete melting of the snowpack). They also concluded that the snow cover might migrate northward in future due to warming. In a recent study, Grogan et al. (2020) also documented similar conclusions. However, either lack of domain coverage or analysis of limited variables remain a hindrance in comprehensive understanding of the regional hydrologic changes in NEUS.

The extent of inland flooding and surface water depths resulting from the extreme flood events are also likely to change in future. However, this has not been investigated yet; perhaps due to limited availability of observations and modeled flood elevation estimates (Wobus et al., 2021; Collins et al., 2022). Besides, previous studies over NEUS have focused on the hydrologic conditions of individual river basins at coarse resolution. Hence, precise changes in spatial patterns of such hydrologic changes remain unexplored.

Global Climate Models (GCMs) are widely used tools to simulate the response of global climate to increasing greenhouse gas (GHG) concentrations. However, most of the current GCMs are coarse-resolution (hundreds of kilometers) and are often unable to reproduce climatic and weather features at regional or local scale. To overcome this, regional climate models (RCMs) are used in conjunction with GCMs to dynamically downscale the projections for a specific region (Castro et al., 2005; Pal et al., 2019; Kotamarthi et al., 2021). To assess the hydrologic impacts of climate change, previous studies have used several GCM-downscaled climate products under various Representative Concentration Pathway (RCP) scenarios to force the hydrologic models (Sunde et al., 2017; Quansah et al., 2021). For this study, we use the Weather Research and Forecasting (WRF) model as RCM to dynamically downscale decade long GCM climate projections for 'Historic' (1995-2004) and 'Future' (2045-2054) periods under RCP8.5 scenario at a spatial resolution of 12km. Next, we implement WRF's high-resolution distributed hydrologic modeling component WRF-Hydro for the hydrologic modeling purposes. WRF-Hydro is currently the underlying framework for the National Water Model of the US and is capable of simulating the entire hydrologic cycle at a local to neighborhood scale. WRF and WRF-Hydro ensures a highly resolved climate forcing and detailed representation of heterogeneous topographical features as opposed to previously performed coarse-resolution macro scale modeling studies (Demaria et al., 2016a; Naz et al., 2016) performed over NEUS. Somos-Valenzuela and Palmer (2018) used WRF-Hydro to calculate historical water budget tendencies over NEUS watersheds. This modeling approach also generates unique high-resolution inland flooding water depth maps at high spatiotemporal resolution along with the conventional hydrologic modeling outputs, such as streamflow, snowpack, soil moisture, and evapotranspiration. However, due to its high computational cost for large domains, most studies have used it over a watershed scale and focus on short-term events. Our study is first of its kind to provide extreme inland flood magnitudes and extent estimates of the past and future decades at a high resolution of 200 meters over the entire NEUS of 1380 x 1320 km^2. Furthermore, we developed stationary and non-stationary extreme value analysis parameters over NEUS to calculate return levels with uncertainty estimates at any given return period. We also provide a comprehensive overview of other hydrologic changes over the entire NEUS to understand the changes in water balance and the potential drivers of the changes in streamflow and inland flooding, which also help reinforce some of the conclusions found in previous literature.

The main goals of this study are to: (1) Investigate the changes in the hydrologic conditions in terms of streamflow, ET, soil moisture and snowpack amount of the entire NEUS and validate with previous regional scale studies with different model combinations. (2) Quantify changes in inland flood magnitude and extent in near future. (3) Use Generalized Extreme Value (GEV) theory to predict risks and associated uncertainty of the low-frequency events.

The paper is organized as follows: in Section 2, the study region, data and methods are discussed. Section 3 describes the results and finally, a summary and the conclusions are documented in Section 4. Additional information is provided in Supporting Information (SI).

2 Materials and Methods

2.1. Study region

NEUS is a region where strong evidence of increased extreme precipitation intensity has been observed in the 20th century (Brown et al., 2010; Guilbert et al., 2015, Zobel et al., 2018a). NEUS is one of the most developed areas in the world with more than sixty-four million people living there. Hence, the watersheds are under the influence of anthropogenic activities like land use and land cover change, water regulations, population growth etc. Such anthropogenic activities on top of climate variabilities pose a threat to flow regimes and inland flooding conditions of the NEUS watersheds (Siddique et al., 2021).

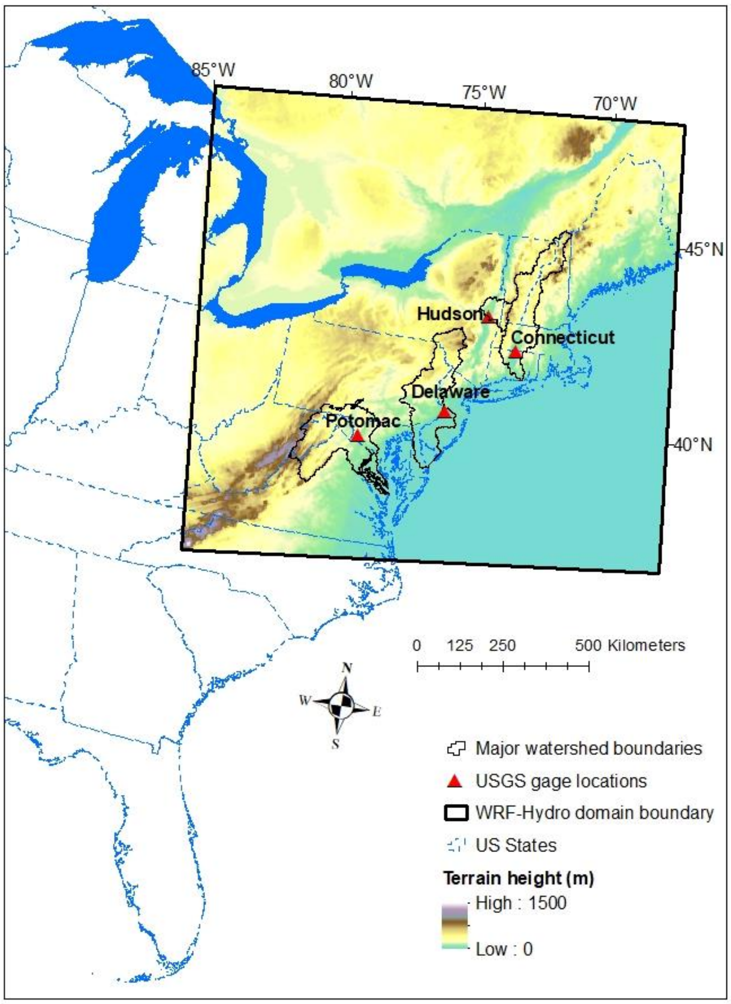

Figure 1. NEUS WRF-Hydro domain on the US map with the major watersheds and USGS gages marked. Topography (terrain height in meters) is shown with shading.

This study includes the states: Maine, Vermont, New York, New Hampshire, Massachusetts, Rhode Island, Connecticut, New Jersey, Delaware, Maryland, Pennsylvania, Virginia, and West Virginia (Figure 1) covering entire 'New England' (HUC01) and 'Mid-Atlantic' (HUC02) hydrologic units (Seaber et al., 1987). As such, the WRF-Hydro domain (35N-50N, 65W-85W) includes all the major rivers in this region: Connecticut, Hudson, Delaware, Potomac, Merrimack, and Susquehanna. Two rivers from northern part – Connecticut (United States Geological Survey

[USGS] gage ID 0118400) and Hudson (USGS gage ID 01335754), and two rivers from the southern part- Delaware (USGS gage ID 01463500) and Potomac (USGS gage ID 01638500) were analyzed in this study. The watersheds and the USGS gages considered for this study are highlighted in Figure 1. We selected the gages with natural flow on the major rivers based on complete data availability within the historic period. Gages with influences of dam were not considered due to limited representation capability of reservoirs in the hydrologic model. December to February (DJF), March to May (MAM), June to August (JJA) and September to November (SON) are considered as winter, spring, summer and fall in NEUS, respectively.

2.2. Dynamically downscaled RCM outputs

We used WRF v3.3.1 model (Skamarock et al., 2008) to dynamically downscale three sets of Coupled Model Intercomparison Project 5 (CMIP5) GCMs: Community Climate System Model 4 (CCSM4, Gent et al., 2011), the Geophysical Fluid Dynamics Laboratory Earth System Model 2 (GFDL-ESM2G, Donner et al., 2011), and the Hadley Centre Global Environment Model version 2 (HadGEM2-ES, Jones et al., 2011). These GCMs were found suitable to represent the spread of climate sensitivity for the 30 GCMs in the CMIP5 experiment (Sherwood et al., 2014). The corresponding downscaled products are referred to as CCSM-WRF, GFDL-WRF and HadGEM-WRF hereafter. In both CCSM-WRF and GFDL-WRF, boundary conditions are bias-corrected using reanalysis data; and nudging techniques are applied to WRF runs (Wang and Kotamarthi 2015). No bias-correction or nudging are applied to the HadGEM-WRF. The WRF domain covered most of North America with 12-km grid spacing. Detailed description of the WRF model set up and RCM simulations can be found in Zobel et al. (2018a) and Pringle et al. (2021). Each RCM provides dynamically downscaled estimates of two decadal periods 1995-2004 ('Historic' hereafter) and 2045-2054 ('Future' hereafter) with one-year spin-up time for each period (1994 and 2044) which are excluded for analysis. The future projections were conducted under RCP 8.5 assuming business-as-usual, as it accurately represents current emissions out until mid-century (Schwalm et al., 2020). Output from the WRF simulations at 3-hourly intervals were regridded to 4 km and used to force the hydrologic model WRF-Hydro. The precipitation was bias-corrected (see section 2.3) before regridding.

2.3. Bias correction of precipitation

The WRF precipitation projections were bias corrected with hybridized quantile mapping technique, which isolates extremes from the lower quantiles to identify and correct biases separately. The extremes were determined based on top 2% precipitation as points over threshold (POT). The Generalized Pareto (GP) cumulative distribution function (CDF) identifies quantiles in the observed and modeled POTs (for the same reference period) that are equivalent to those in the future projected POT. The future projections were then adjusted by the ratio of the observed to the modeled reference POT as a scaling factor at each quantile with the following equation:

$$\mathrm{POT_c} = \mathrm{POT_{fut}} * \frac{\mathrm{F^{-1}_{GP,obs}}\left(\mathrm{F_{GP,fut}}(\mathrm{POT_{fut}})\right)}{\mathrm{F^{-1}_{GP,hist}}\left(\mathrm{F_{GP,fut}}(\mathrm{POT_{fut}})\right)}$$

where $\mathrm{POT_c}$ is bias corrected future POT, $\mathrm{POT_{fut}}$ are the modeled future POT, $\mathrm{F_{GP,fut}}$ is the GP CDF for the modeled future POT, and $\mathrm{F^{-1}_{GP,obs}}$ and $\mathrm{F^{-1}_{GP,hist}}$ are the inverse GP CDFs for the observed and modeled reference POT, respectively.

The lower 98% of precipitation as points under threshold (PUT) were split into four subsets by seasons, and each was corrected in a similar way according to the equation:

$$\mathrm{PUT_c} = \mathrm{PUT_{fut}} * \frac{\mathrm{F^{-1}_{emp,obs}}\left(\mathrm{F_{emp,fut}}(\mathrm{PUT_{fut}})\right)}{\mathrm{F^{-1}_{emp,hist}}\left(\mathrm{F_{emp,fut}}(\mathrm{PUT_{fut}})\right)}$$

where $\mathrm{PUT_{fut}}$ are the modeled future PUT for a given seasonal subset, $\mathrm{F_{emp,fut}}$ is the empirical CDF for the modeled future PUT, and $\mathrm{F^{-1}_{emp,obs}}$ and $\mathrm{F^{-1}_{emp,hist}}$ are the inverse empirical CDFs for the observed and modeled reference PUT, respectively. The $\mathrm{PUT_c}$ are the corrected PUT precipitation for a given season.

The bias correction was explicitly performed based on the daily data. The corrected daily precipitation was temporally downscaled to 3-hourly values using the same temporal distribution for each day projected by the model.

2.4. WRF-Hydro and Calibration

The bias corrected precipitation along with other WRF meteorological forcing (specific humidity, air temperature, incoming shortwave radiation, incoming longwave radiation, surface pressure, and near surface wind) were used every 3-hour to force the hydrologic model WRF-hydro in standalone mode. WRF-Hydro 5.1.1 (Gochis et al. 2020; Pal et al., 2021a) is a physics-based, parallelized, distributed hydrologic model. It was set up using multiple grid structures in the basin, such that the Noah-MP land surface model ([LSM], Niu et al., 2011; Pal et al., 2021b) operated at 4-km horizontal grid spacing with an additional representation of overland flow, along with channel routing on a 200-m grid (aggregation factor of 20) to accurately represent the river network of NEUS. A 90-m digital elevation model (DEM) was incorporated to create this routing grid using WRF-Hydro GIS Pre-processing Toolkit v5.1.1. Our domain contained 6880 west-east x 6580 north-south grid cells. Surface flow, saturated subsurface flow, gridded channel routing, and a conceptual baseflow ("pass-through") were active during the simulations. The time steps for Noah-MP, channel routing, and terrain routing were 60 minutes, 20 minutes and 10 seconds, respectively. Six decadal continuous hydrologic simulations were conducted (Table 1) with a similar model set up, except the climate forcing, to identify the changes in hydrologic condition due to climate change projected by different GCMs. The 'Historic' simulations started on January 1, 1995 and continued till December 31, 2004. The 'Future' simulations started on January 1, 2045 and continued till December 31, 2054. All these simulations were 'warm-started' from similar

Table 1. Hydrologic simulations conducted in this study using WRF-Hydro standalone mode, driven by WRF outputs.

Simulation name	Simulation year	Forcing
CCSM-Hydro-Historic	1995-2004	CCSM-WRF
CCSM-Hydro-Future	2045-2054	CCSM-WRF
GFDL-Hydro-Historic	1995-2004	GFDL-WRF
GFDL-Hydro-Future	2045-2054	GFDL-WRF
HadGEM-Hydro-Historic	1995-2004	HadGEM-WRF
HadGEM-Hydro-Future	2045-2054	HadGEM-WRF

initial conditions after six months of model spin-up. Model LSM outputs (including ET, snow water equivalent and soil moisture) were saved every 6-hour and routing outputs (including streamflow and surface water depth) were saved every hour. Multi-model averages (MMA) are often used in this study to demonstrate the results, which helps to reduce the variability coming from individual models.

USGS discharge data at the four major river locations (Figure 1) were used to calibrate and validate the performance of WRF-Hydro. The stations on these major rivers were chosen based on the available data record for 1995-2004 and avoiding any flow with dam interference. Since this study focuses on hydrological extremes which is more important than moderate and low quantities when estimating the resulting risks, event-based model calibration is performed for two major extreme rainfall events of 1995 using Parameter Estimation Tool (PEST) following Wang et al. (2019). The calibration simulations were performed for 3 days (after six months of spin-up) with 120 parallel simulations to calibrate a total 22 model parameters (See Table S1 in SI) on a high-performance computing (HPC) system. The forcing used for calibration came from North American Land Data Assimilation System (NLDAS2 [Xia et al., 2012]).

2.4.1. Inland flooding in WRF-Hydro

The LSM within WRF-Hydro calculates the fluxes of moisture and energy. Infiltration excess, ponded water depth and soil moisture are subsequently disaggregated from the LSM grid (here 4 km) to the routing grid (here 200m) using a time-step weighted method (Gochis and Chen, 2003) and are passed to the overland and subsurface terrain-routing modules (Gochis et al., 2020). Depth of surface head (or ponded water) on any grid cell is a combination of the local infiltration excess, the amount of water flowing onto the grid cell from overland flow, and exfiltration from groundwater flow, and is saved as one of the hourly outputs in WRF-Hydro (variable 'sfcheadsubrt'). After the execution of routing schemes these fine-grid values are aggregated back to the native land surface model grid as 'sfcheadrt' and used on the next iteration as:

$$sfcheadrt_{i,j} = \frac{\sum\sum sfcheadsubrt_{irt,jrt}}{AGGFACTRT^2}$$

where (irt, jrt) are the grid cells within native grid cell (i, j) and AGGREFACTRT is the aggregation factor. We can use the variable 'sfcheadsubrt' (mm) as a proxy for inundation, with nonzero values indicating wet land surfaces. However, we acknowledge that the depths might be slightly off from actual inundation at local scales, partially because of the small size of the grid cells and the coarseness of the DEM at that scale. In addition, WRF-Hydro does not explicitly represent inundation areas from overbank flow as water does not flow from any channel back to the terrain. Hence, we consider non-channel overland flow or local ponding depth as inland flood depth in this study.

2.5. Extreme value analysis and uncertainty quantification

Extreme value analysis (EVA) is performed to estimate intensities of extreme climate and hydrologic events from annual maximum series (AMS) isolated from the 'Historic' and 'Future' simulations. The CDF of the GEV distribution is given by:

$$F(x; \mu, \sigma, \xi) = \exp\left\{-\left[1 + \xi\left(\frac{x-\mu}{\sigma}\right)\right]^{-1/\xi}\right\}$$

with parameters μ (location), σ (scale), and ξ (shape). For a stationary GEV all parameters are considered constant. Where the distribution of extreme events is expected to change over time, one or more parameters of the GEV may be defined as time variant(s). In this study, for a non-stationary GEV the location parameter is modeled as a first-degree linear function of time.

For historical EVA the stationary GEV is used. For the 'Future' scenario, either the stationary or non-stationary GEV is chosen via the log-likelihood ratio test. To account for numerical instabilities in the WRF-Hydro simulations while fitting the GEV, only points with sufficient data above a 0.3 mm (0.001 ft) threshold are considered. In the historic analysis, sufficient data is defined as 8 years of annual maximums above the threshold. In the combined 'Historic' and 'Future' analysis, 16 years of data above the threshold is used to define data sufficiency. Each year included in the analysis was required to have at least 2 models with adequate data. Extreme inland flood and flow events are calculated at 2-, 5-, 10-, 25-, and 50-year return periods by calculating the respective percentiles of the fitted distribution's CDF at each cell.

One consideration in estimating extreme event intensities is the varying range of climate variables forecasted by the three WRF simulations used in this study. To quantify the uncertainties of extreme climate events, statistical bootstrapping is used to generate a pool of 500 augmented AMS. In each augmented AMS, annual maxima are randomly sampled from the AMS isolated from 3 the RCMs. Stationary and non-stationary GEV are fit to each AMS, and the 5th, 50th, and 95th percentiles of 500 GEV returns are used as lower, median, and upper bounds for extreme event estimates.

3. Results and discussions

3.1. Validation of WRF and WRF-Hydro model

The WRF simulations used in this study have been evaluated extensively (Wang and Kotamarthi 2015; Chang et al. 2016, Zobel et al. 2017, 2018a; Pringle et al. 2021). Here we evaluate the performance of WRF-Hydro when forced with WRF outputs and bias corrected downscaled

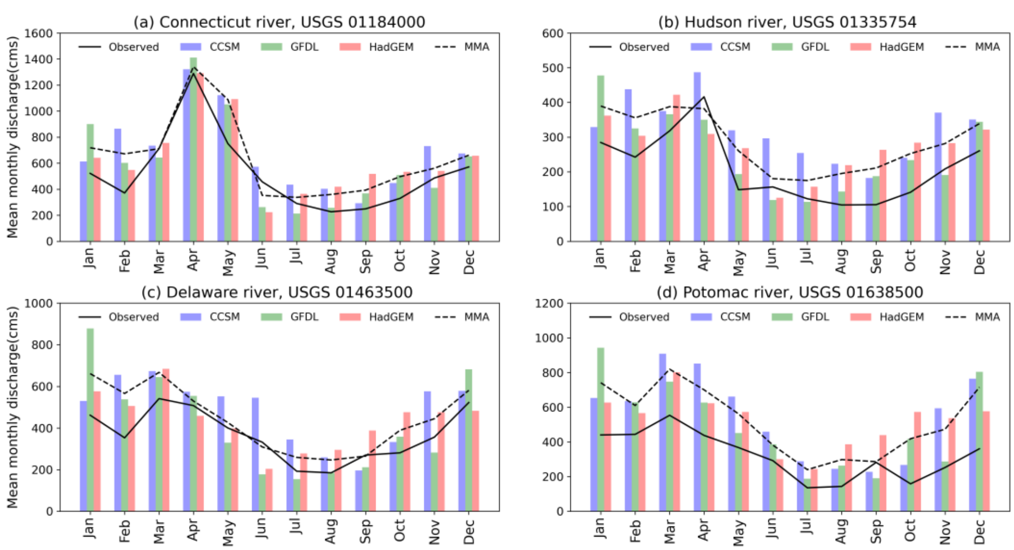

Figure 2. Comparison of WRF-Hydro simulated historical river discharge to USGS observed discharge over the four sites shown in Figure 1. The three model estimates are shown in colored bars, USGS data is shown in solid black lines, multi-model average (MMA) is shown in black dashed line. CCSM = CCSM-Hydro-Historic, GFDL = GFDL-Hydro-Historic, HadGEM = HadGEM-Hydro-Historic.

precipitation estimates. We compare the model simulated monthly streamflow at the major river locations and demonstrate that the hydrologic model represents the seasonality and magnitude of mean monthly flow well (Figure 2). The temporal correlation of MMA and observed was found 0.92, 0.89, 0.88 and 0.89 in Connecticut, Hudson, Delaware, and Potomac, respectively. However, there are some overestimations for the majority of the months in all the locations (except some of the summer months for GFDL and HadGEM). This could be expected as we calibrated the model with respect to high-flow events. However, since we use the same calibrated parameters for the 'Historic' and 'Future' scenario, the effect of the bias on the changes is expected to be minimal. All the rivers achieve peak flow in March-April and low flows in the summer (JJA). Connecticut river, the longest stream in New England, has the highest discharge reaching up to mean monthly discharge of 1200 cubic meters per second (cms) in April.

3.2. Changes in precipitation

Figure 3 shows the changes in decadal mean precipitation and decadal maximum precipitation. Overall, the projected changes in decadal mean are smaller compared to the changes in the extremes. The decadal mean precipitation changes (Figure 3a-3d) are within 25%, whereas changes in decadal maximum precipitation are likely to exceed 100%. While all the three models show similar magnitude in the changes of mean and maximum precipitation, the location of these changes remains uncertain. For example, CCSM-WRF and GFDL-WRF (Figure 3a, b) project majorly positive changes in the decadal mean precipitation, but HadGEM-WRF (Figure 3c) predicts both negative and positive mean changes. Nonetheless, profound changes in decadal maximum precipitation are likely to be positive. Future extreme precipitation is projected to increase more than 100% in southern NEUS by CCSM-WRF; parts of New York, Pennsylvania

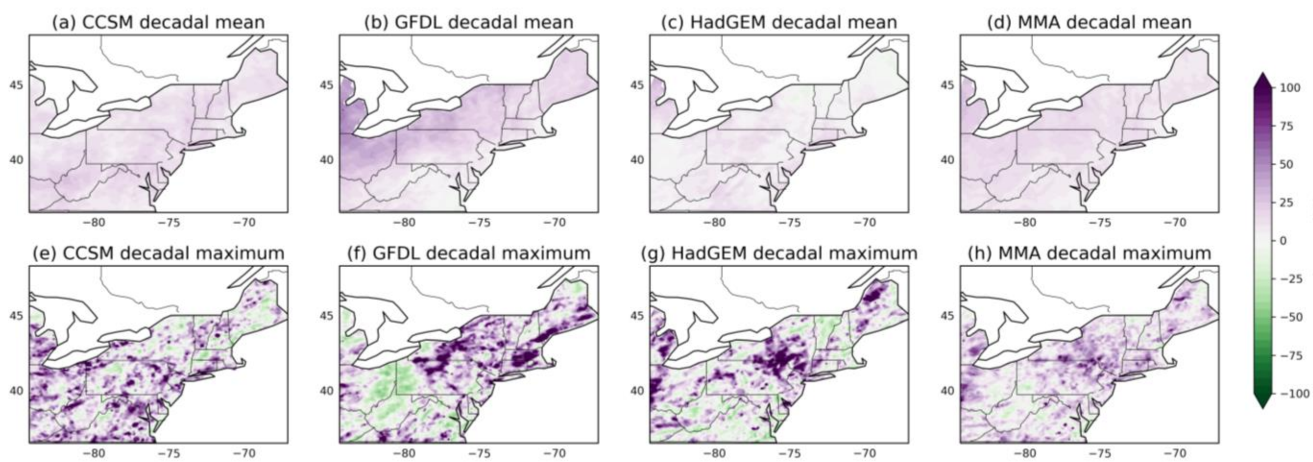

Figure 3. Changes in decadal mean (top row) and decadal maximum (bottom row) precipitation as projected by CCSM-WRF (a, d), GFDL-WRF (b, e) and HadGEM-WRF (c, f). Multi-model average is shown in (d) and (h) for mean and maximum precipitation, respectively.

and Maine by GFDL-WRF and HadGEM-WRF (Figure 3e, 3g). Additionally, GFDL-WRF predicts similar large changes in Massachusetts and Connecticut as well (Figure 3f). The MMA estimate of extremes (Figure 3h) reduces some of the high variability and predicts ~ 75% increase in some regions of New York and Pennsylvania. In-depth discussions on changes in extreme precipitation can be found in Zobel et al. (2018b). Here we focus on the effects of such precipitation changes on the surface hydrology.

3.3. Changes in Streamflow

Relative changes in monthly streamflow between 'Historic' and 'Future' simulations are shown in Figure 4. Left (right) column demonstrates the changes in mean (extreme) flow. The relative changes for mean flow range between -20% to 40%, with decreases in the summer and late spring and increases in winter and early spring. Fall discharge is projected to increase in the southern watersheds (Delaware and Potomac) and decrease in the northern watersheds (Connecticut and Hudson). These results are consistent with previous studies (Parr et al., 2015b; Siddique et al., 2021), indicating that the watersheds of NEUS are moving towards a wetter regime particularly during the months of winter, along with a drier summer season. Future increases in temperature (Figure S1 in SI) allows the atmosphere to hold more moisture, which results in an increase of precipitation in most of the months of the year (Figure S2). Snow also plays a critical role in this region as snowmelt contributes to the seasonal flow. With higher temperature, less available snowpack (see Figure S3 and Figure 8) and faster snowmelt will result in an increase in flow in

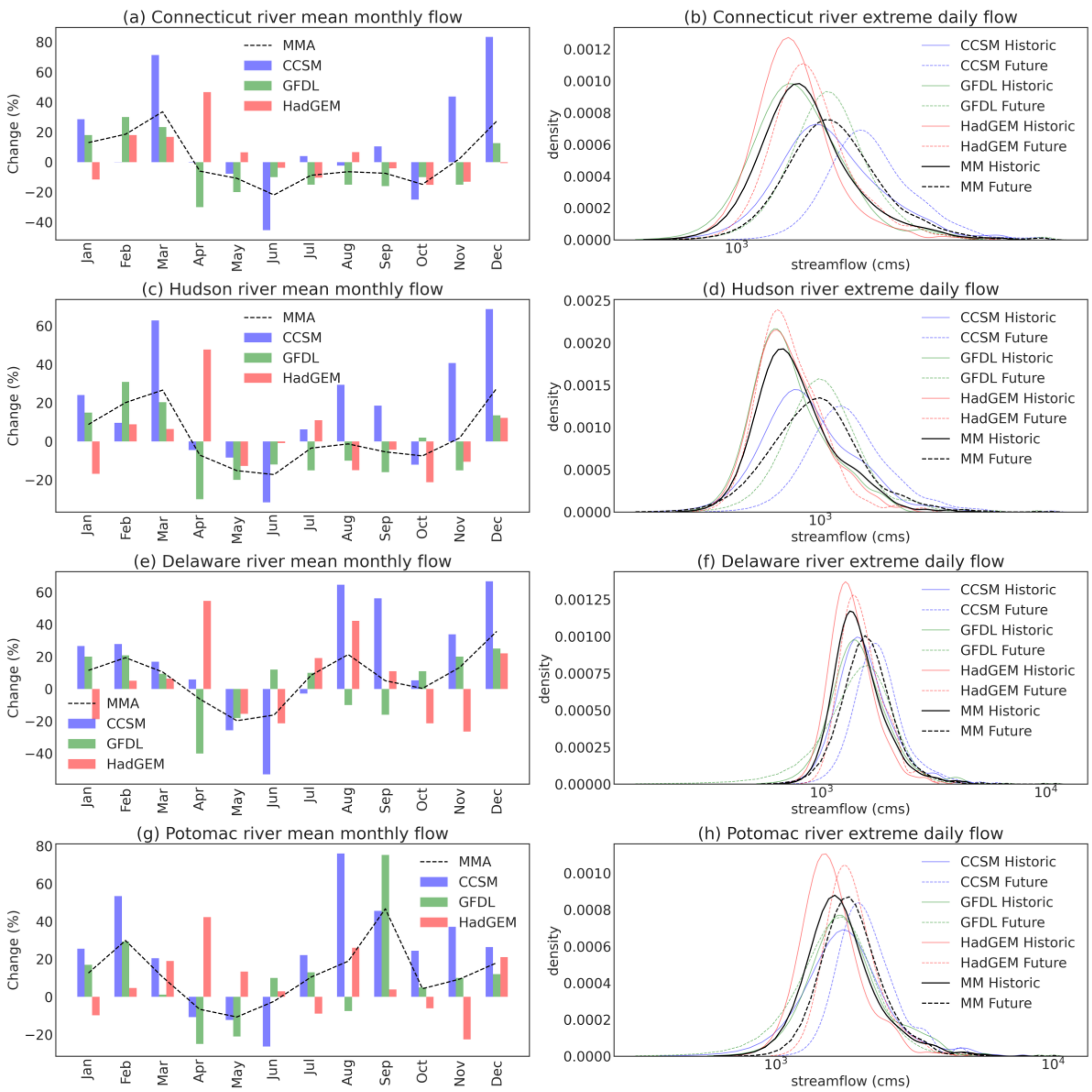

Figure 4. Percentage changes in monthly streamflow in the rivers of NEUS (left column), and changes in the distribution of extreme flows (right column). MMA = multi-model average. CCSM = CCSM-Hydro, GFDL = GFDL-Hydro, HadGEM = HadGEM-Hydro.

early spring and decrease in late spring.

Consensus among the three models is seen in the distributions of extreme flow (>95 percentile) shown in the right column of Figure 4. The distributions shift towards the right in future, indicating higher mean intensity of extreme flows in future. The extreme flows in these rivers are mostly observed in winter and spring. Combined modeled (MM, black dashed lines) flows indicate the mean of the extreme flow is predicted to increase by ~20% in Connecticut and Hudson river (Figure 4b, d), 10.5% in Delaware (Figure 4f) and 5.1% in Potomac river (Figure 4h).

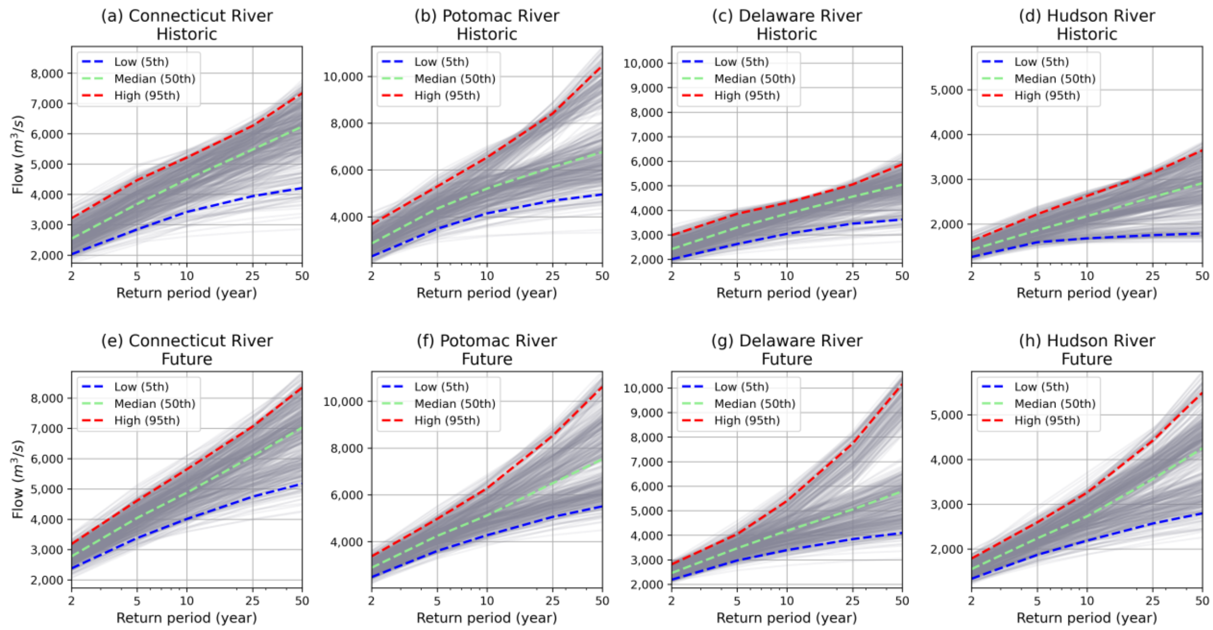

Figure 5. GEV projected flow in the rivers for (a-d) 1995-2004 historic and (e-h) 2045-2054 mid-century scenario.

Table 2. EVA projected future changes in extreme precipitation (P) and streamflow (Q) at the four major river basins.

	2-year event		**5-year event**		**10-year event**		**25-year event**		**50-year event**	
	P	**Q**	**P**	**Q**	**P**	**Q**	**P**	**Q**	**P**	**Q**
Connecticut	8.1%	9.2%	8.5%	9.9%	9.2%	8.4%	10.5%	11.1%	12.1%	12.7%
Potomac	4.1%	1.2%	4.1%	-2.4%	4.8%	-1.7%	5.9%	6.1%	7.1%	11.2%
Delaware	8.2%	1.7%	9.1%	5.1%	10.3%	8.4%	12.7%	10.8%	14.7%	14.8%
Hudson	10.5%	8.8%	12.4%	20.1%	13.9%	25.5%	16.1%	36.8%	17.9%	45.8%

Figure 5 shows the return level of streamflow for different return periods based on the re-sampled lower, median and higher quantities of streamflow over each of the four rivers (see section 2.5). Overall, the changes were prominent in the low-frequency events, such as the once-every-50-year events (Figure 5). For example, based on the resampled median quantities, 50-year flow magnitude increased from 6240 to 7030 m^3/sec in Connecticut river (Figure 5a, e), 5040 to 5800 m^3/sec in Delaware river (Figure 5c, g), 2900 to 4250 m^3/sec in Hudson river (Figure 5d, h), and 6750 to 7520 m^3/sec in Potomac river (Figure 5b, f). 5^{th} and 95^{th} quantiles of the uncertainty bounds were also plotted to incorporate the inter-model spread (see section 2.5). We conclude that the changes in extreme precipitation over these watersheds are the main drivers for such changes in extreme flow. Table 2 demonstrates a complete picture of the percent changes in the risks associated with precipitation and flow coming out from those watersheds. We expect positive changes in extreme precipitation contributing to extreme flows, except 5-year and 10-year events in Potomac river where streamflow may decrease even with an increase in precipitation extreme.

3.4. Changes in inland flooding

This study highlights the capability of WRF-Hydro in simulating and projecting changes in inland flooding conditions over the NEUS. In WRF-Hydro, inland flooding can be assessed in terms of the extent and depth of surface water accumulation (see section 2.4). We analyze combined multi-model estimates instead of individual models using the resampling approach (section 2.5). The results indicate more inundation areas and increased intensity of extreme

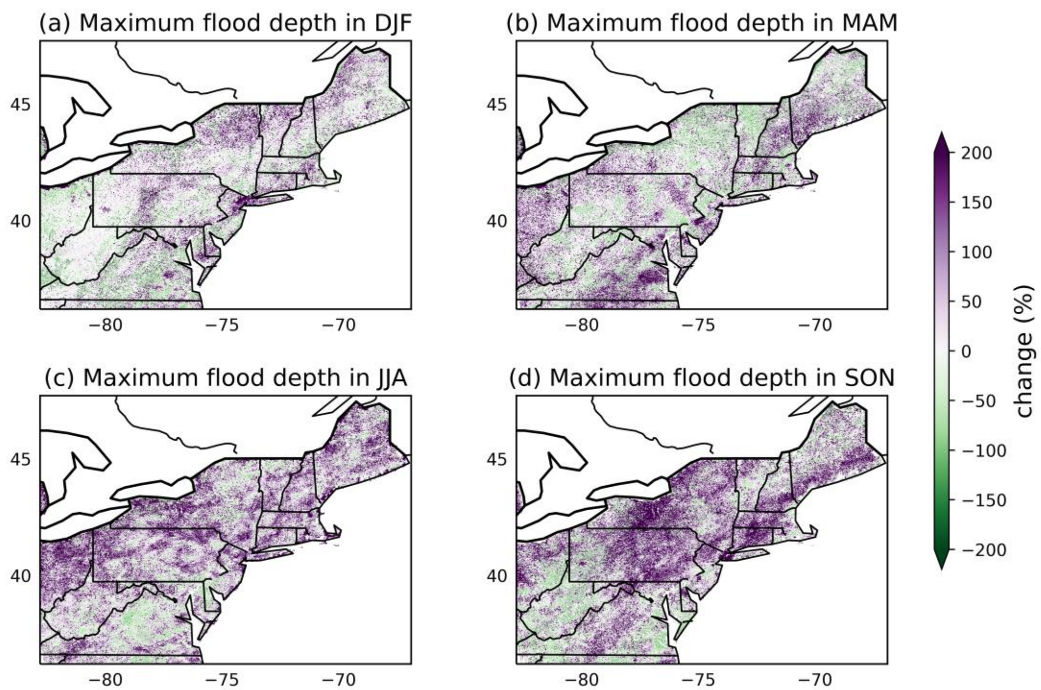

Figure 6. Projected percent changes in 10-year seasonal maximum surface water depth at grid spacing of 200 m based on three model averages.

inland floods (measured by mm of water) in the NEUS by mid-century. Figure 6 demonstrates the predicted changes in maximum flood depth in each season. Highest changes are seen in summer (JJA) and fall (SON), likely due to the increases in extreme precipitation and tropical-to-extratropical cyclone activities over the Atlantic coast in these months in future (Garner et al., 2021; Gori et al., 2022). Regions in New York, Connecticut, Massachusetts and New Hampshire may experience a change of ~200% (Figure 6c, d). Winter (DJF) and spring (MAM) changes range 50-100% in the states of Virginia, New Hampshire and Maine.

According to the GEV analysis, likelihood and flood severity of extreme low-frequency flood is expected to increase. Figure 7 shows the map of 2-year (a, b) and 50-year events (c, d) for historic and mid-century periods. Water depth from high-frequency flooding may increase from 60 mm (2.4 inches) to 100 mm (4 inches) in all states (Figure 7a, 7b). Low-frequency extreme events may cause accumulated water depths of >350 mm (1.15ft) in regions of Pennsylvania and Ohio which were not seen in the historic scenario. Predicted hotspots are in west Vermont, southern New York and Connecticut as well (Figure 7c, 7d). In terms of spatial extent, total flooded area is projected to increase by 20% for all return periods (Figure 7e). In general, higher percent increases can be expected in the grid cells with higher water depth, except >300mm grid cells in the 2-year return period (Figure 7e). This suggests that extreme inland flooding might be occurring in more regions than historic scenarios.

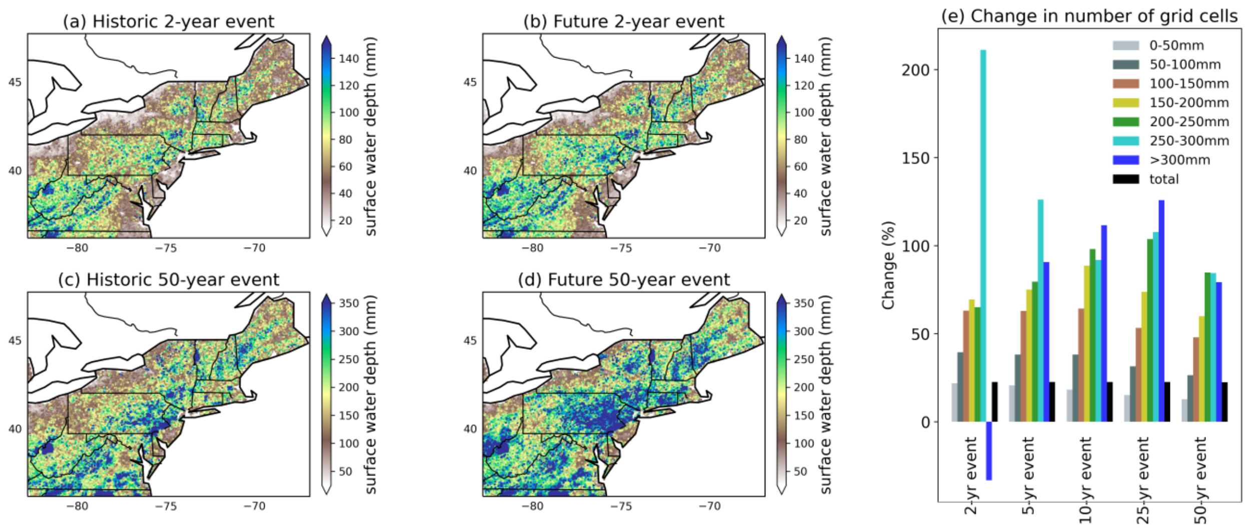

Figure 7. GEV projected inland flooding estimates of 2-year (top row) and 50-year (bottom row) events for 1995-2004 (a, c) and 2045-2054 (b, d). (e) Change in number of wet grid cells according to surface water depth.

Furthermore, we were able to investigate the changes in inland flooding at a local scale or neighborhood level with the help of high-resolution modeling. Figure 8 demonstrates some examples of changes around a few major cities of NEUS – Philadelphia (Figure 8a, b), New York (Figure 8c, d), Boston (Figure 8e, f) and Washington D.C (Figure 8g, h). In general, lower flood intensity grids (colorless dots) are predicted to decrease and higher flood intensity grids (blue and red) are predicted to increase in number. Especially in the areas surrounding New York, there was a significant increase in the number of flooded grids projected by GEV analysis. The estimates at 200m resolution are available (see 'Data availability statement') for understanding flood risk at a local scale anywhere in the study domain.

3.5. Changes in mean ET, Soil moisture and SWE

Projected changes in precipitation and flow are linked to the other hydrologic variables over NEUS such as ET, soil moisture, and SWE, which are provided by the output of LSM component of WRF-Hydro (i.e. Noah-MP). Due to consistent warming in NEUS (supplementary Figure S1), larger portion of winter precipitation falls as rainfall, with decreased SWE, and higher snowmelt in most of the parts of NEUS, especially in the watersheds of concern (Figure 9a-9d), leading to higher runoff in winter. In NEUS rivers, peak flows generally occur during March-April when snowmelt is triggered by temperature increase. Hence, earlier peak snowmelt will likely cause an earlier peak in river flow (Figure 4, supplementary Figure S3).

Changes in soil moisture can cause infiltration and surface runoff change. We find a domain-wide decrease in JJA soil moisture (Figure 9g), over the northern part in SON (Figure 9h), causing

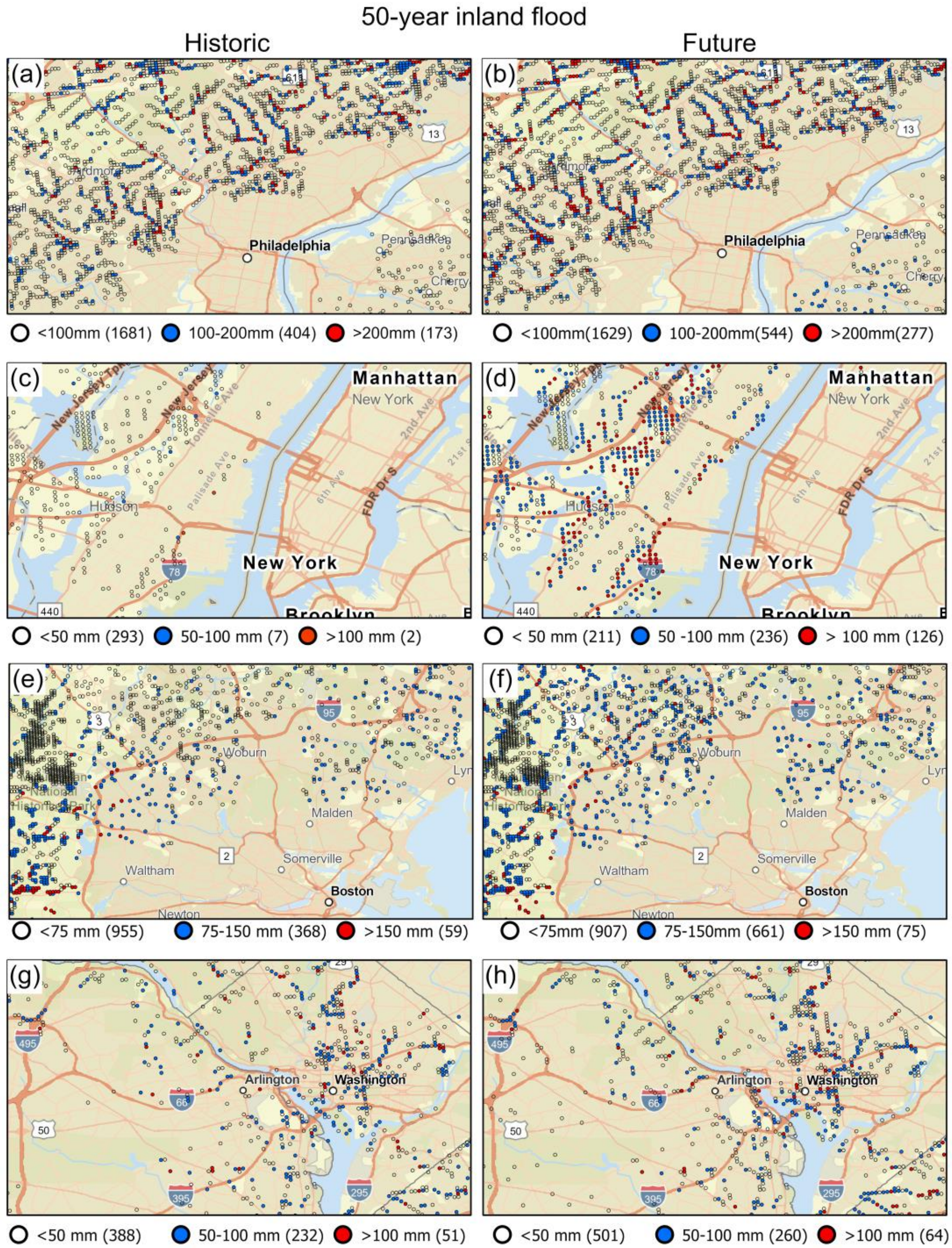

Figure 8. Extreme surface water depths (mm) in a 50-year event around major cities of NEUS – (a, b) Philadelphia, (c, d) New York, (e, f) Boston and (g, h) Washington D.C in Historic and Future scenario. Total number of grid cells counted in each category are also mentioned in parentheses.

more infiltration and less surface runoff, which explains the decrease in summer flow in the rivers and decrease in spring flow in northern watersheds (Figure 4). Increase in soil moisture in DJF and MAM (Figure 9e, 9f) is likely due to increased precipitation and snowmelt. The range of mean soil moisture change stays within ±5%.

ET amount depends on surface energy budget and available energy, which creates evaporative demand. As the temperature rises in the future (Figure S1), ET is also expected to rise if moisture is available. Our simulations indicate an increase of ET throughout all four seasons in the mid-century (Figure 9i-9l) with the highest increase in JJA (Figure 9k). Future rise in temperature and precipitation causes a domain-wide increase of ET ~10%. It is worth mentioning here that the accuracy of ET estimates in a land surface model depends on accurate land classification and ET-related parameter tuning (Pal et al., 2021b). In this study we did not modify any land related model parameters for future projections to attribute the changes to climate change only.

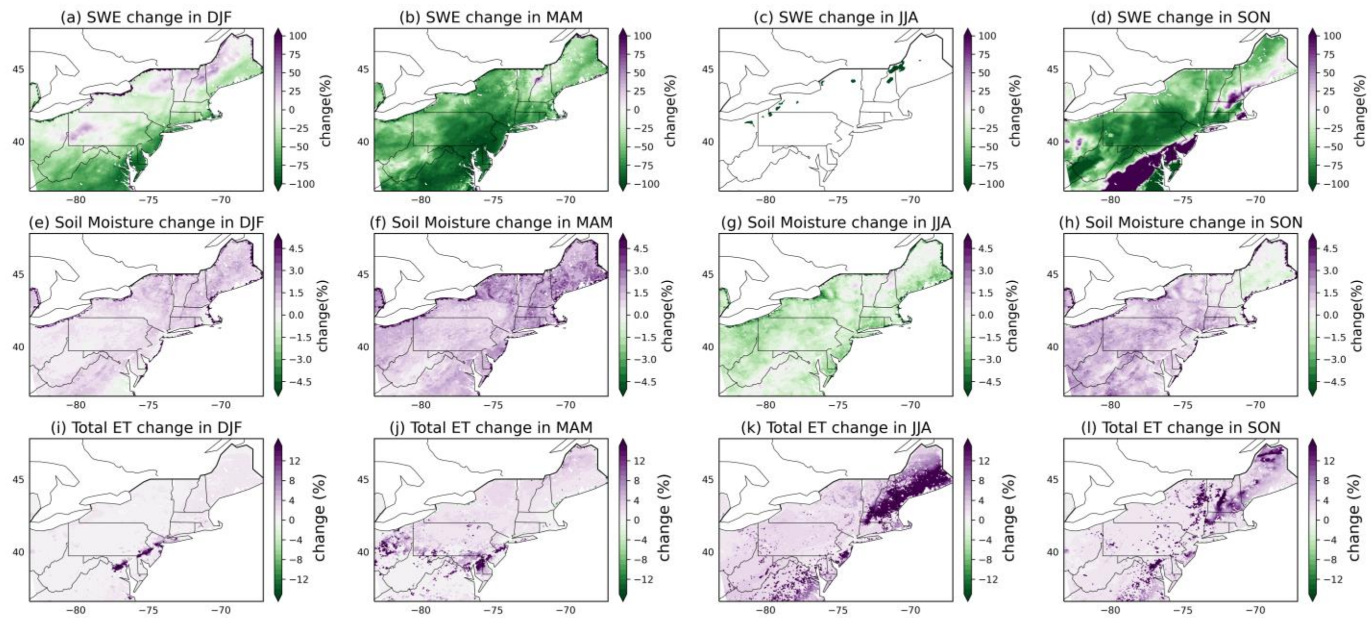

Figure 9. Multi-model average seasonal percent changes in snow water equivalent (SWE), total evapotranspiration (ET) and soil moisture.

4 Summary and conclusions

Climate change has significant impacts on the hydrologic cycle as a warming atmosphere influences the patterns of extreme precipitation and alters regional flood risks. Assessing such impact at regional to neighborhood scale is necessary for decision making and developing mitigation strategies. Different agencies are now considering climate change policies for adaptation and asset management purposes as extreme precipitation and flooding can pose significant risks to their infrastructures and networks. In this study, we use high-resolution physics-based models and statistical techniques to quantify increases in hydrologic extremes and predict increased risks in the near-future over the NEUS.

Starting from coarse-resolution global models, we estimated atmospheric forcing at 12-km resolution using WRF. Then the land surface model was run at 4-km and WRF-Hydro hydrologic routing was performed at 200-m resolution. This study is first-of-its-kind to simulate six decade-long hydrologic simulations in such high resolution using 3 million CPU hours of supercomputing resources of Argonne National Laboratory. Total model outputs analyzed were 200 TB. The high spatial resolution generates sufficiently detailed outcomes to inform local decisions, while maintaining statistically robust outcomes needed for extreme value analysis. More specifically, we were able to use the variable 'surface head' from WRF-Hydro to investigate the changes in depths and extent of inland flooding in future. It informs the extent and depth of surface water accumulation of inland flooding. This variable has not been explored yet in the WRF-Hydro literature, but we conclude that a properly calibrated model can provide realistic estimates of inland flooding. This could be useful information for National Water Model product users for investigating local flooding in hydroclimate simulations or short-term inundation from tropical storms. We acknowledge that the main limitation of the study is not being able to incorporate the impact of future land use change with climate and remains a future work.

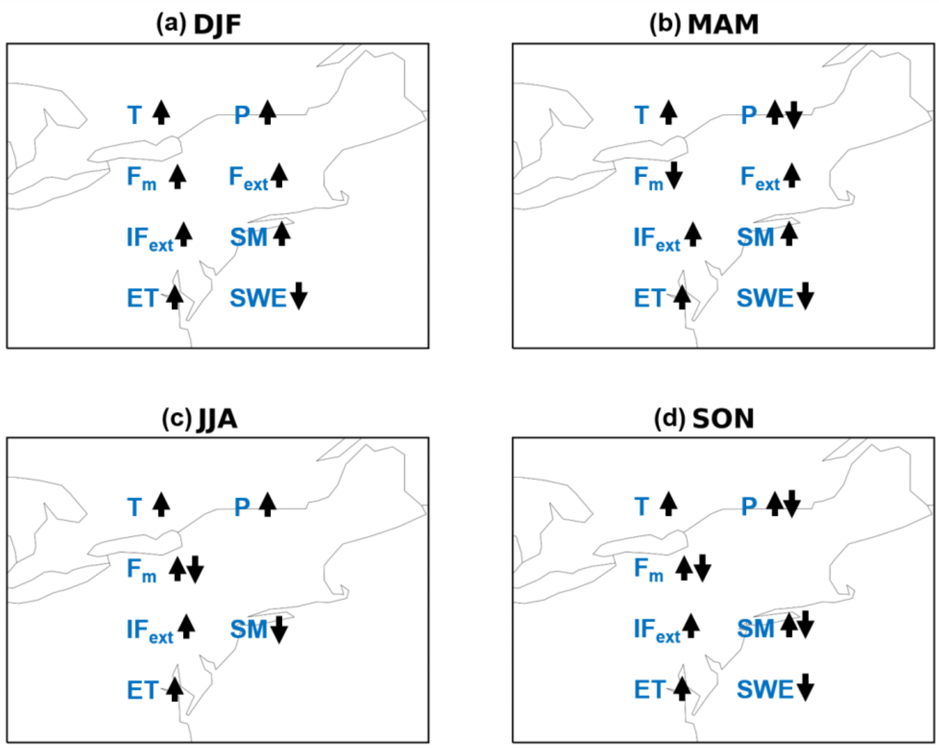

Figure 10. Seasonal changes in the hydroclimatologic variables over NEUS. T = temperature, P = precipitation, F_m = mean flow, F_{ext} = extreme flow, IF_{ext} = maximum inland flood depth, SM = soil moisture, ET = evapotranspiration, SWE = snow water equivalent. Upward (downward) arrow indicates positive (negative) change in future compared to historic. Both arrows indicate both changes were present in either space or time within that season.

Our calculations project that extreme precipitation is likely to increase more (>75%) than mean precipitation (~25%) potentially raising the risk of extreme inland flooding. Increase in mean temperature (Figure S1) likely causes such increases in mean precipitation in most of the months (Figure S2) and increase in ET in all months (since adequate moisture is available). These will also impact other components of the water cycle. In terms of mean monthly flow in the rivers, the expected changes are seasonally varying. In DJF, more liquid rainfall and less snowfall increases the mean and extreme flow, also increasing the soil moisture and maximum inland flood depths. In MAM, faster snowmelt causes earlier peak flow in the rivers but decreases the mean seasonal flow due to less available snowpack. Nonetheless, extreme flow increases due to more water availability. Large temperature increases in JJA cause the largest increase in ET and reduced soil moisture. Mean flow in summer months will likely decrease or increase depending on precipitation variability. As such, a decrease in precipitation in August (Figure S2) might cause flow to decrease in the northern watersheds. However, southern watersheds acquire higher flow due to more rainfall. Similar changes are found in SON where the northern and southern watersheds behave differently. Increase (decrease) in precipitation towards south (north) causes increased (decreased) flow and soil moisture in southern (northern) rivers (Figure 4). Extreme inland flooding is projected to increase throughout the year, especially in JJA and SON due to increase in extreme precipitation. In general, snow water equivalent decreases in all seasons due to substantial increase in temperature. Soil moisture increases in all seasons except summer. Also, northern regions of the NEUS might experience a decrease in soil moisture, which is consistent with the lower SON mean flow there in future. Decrease in soil moisture may have implications for short-term or long-term droughts in NEUS which need further investigation. The seasonal changes are summarized in Figure 10.

GEV estimates indicate correlation between extreme precipitation risk and flow risk. Extreme inland flooding intensity and extent increases throughout the year, especially in the months of JJA and SON. Specifically, more areas of the NEUS are predicted to be affected by low-frequency events in future according to GEV analysis. Total flooded area is projected to increase by 20%. Even the major cities and suburbs will be affected by low-frequency floods of higher return levels. The high-resolution local-scale data is publicly available for further analysis and risk assessment (see the 'Data Availability Statement' section). Our findings from this work are being used by the decision makers of New York Power Authority and AT&T for asset management and adaptation strategies.

Acknowledgments

Support for this study has been provided by the New York Power Authority and AT&T Services Inc. under a Strategic Partnership Project Agreement with Argonne National Laboratory through U.S. Department of Energy contract DE-AC02-06CH11357. We acknowledge the National Energy Research Scientific Computing Center (NERSC), Argonne's Laboratory Computing Resource Center (LCRC), and the Argonne Leadership Computing Facility (ALCF) for providing the computational resources used to conduct the WRF modeling. Similarly, we thank LCRC for providing the computational resources used to conduct the WRF-Hydro modeling in this study. The authors declare no conflict of interest.

Data Availability Statement

NLDAS2 data was downloaded from https://ldas.gsfc.nasa.gov/nldas/nldas-2-forcing-data, WRF-Hydro source code and pre-processing tools were downloaded from https://ral.ucar.edu/projects/wrf_hydro/overview, The observed river discharge is downloaded from the USGS Surface-Water Data website, available at https://waterdata.usgs.gov/nwis/sw (last access: 22 March 2022), streamflow and inland flooding estimates (discussed in Section 3) are available at the Zenodo repository: https://doi.org/10.5281/zenodo.6529651.

References

Allen, M. R. & Ingram, W. J. (2002). Constraints on future changes in climate and the hydrologic cycle. Nature, 419(6903), 224–232. https://doi.org/10.1038/nature01092

Allan, R. P., and B. J. Soden (2008). Atmospheric warming and the amplification of precipitation extremes,Science,321(5895), 1481–1484, https://doi.org/10.1126/science.1160787

Allen, M.R., O.P. Dube, W. Solecki, F. Aragón-Durand, W. Cramer, S. Humphreys, M. Kainuma, J. Kala, N. Mahowald, Y. Mulugetta, R. Perez, M. Wairiu, and K. Zickfeld (2018) Framing and Context Supplementary Material. In: Global Warming of 1.5°C. An IPCC Special Report on the impacts of global warming of 1.5°C above pre-industrial levels and related global greenhouse gas emission pathways, in the context of strengthening the global response to the threat of climate change, sustainable development, and efforts to eradicate poverty [Masson-Delmotte, V., P. Zhai, H.-O. Pörtner, D. Roberts, J. Skea, P.R. Shukla, A. Pirani, W. Moufouma-Okia, C. Péan, R. Pidcock, S. Connors, J.B.R. Matthews, Y. Chen, X. Zhou, M.I. Gomis, E. Lonnoy, T. Maycock, M. Tignor, and T. Waterfield (eds.)]. Available from https://www.ipcc.ch/sr15

Armstrong, W. H., M. J. Collins, and N. P. Snyder (2014), Hydroclimatic flood trends in the northeastern United States and linkages with large-scale atmospheric circulation patterns, Hydrol. Sci. J.,59(9), 1636–1655. http://dx.doi.org/info:doi/10.1080/02626667.2013.862339

Berton, R., Driscoll, C. T., & Chandler, D. G. (2016). Changing climate increases discharge and attenuates its seasonal distribution in the Northeastern United States. Journal of Hydrology: Regional Studies,5,164–178. https://doi.org/10.1016/j.ejrh.2015.12.057

Bose, A. K., Weiskittel, A., Wagner, R.G. (2017). A three decade assessment of climate-associated changes in forest composition across the north-eastern USA. J. Appl. Ecol., 54, 1592–1604. https://doi.org/10.1111/1365-2664.12917

Brown, P. J., R. S. Bradley, and F. T. Keimig (2010). Changes in extreme climate indices for the northeastern United states, 1870–2005, J. Clim.,23,6555–6572. https://doi.org/10.1175/JHM-D-18-0155.1

Byun, K., Chiu, C.-M., & Hamlet, A. F. (2019). Effects of 21st century climate change on seasonal flow regimes and hydrologic extremes over the Midwest and Great Lakes region of the US. Science of the Total Environment,650, 1261–1277. https://doi.org/10.1016/j.scitotenv.2018.09.063

Castro, C. L., Pielke, R. A., & Leoncini, G. (2005). Dynamical downscaling: Assessment of value retained and added using the regional atmospheric modeling system (RAMS). Journal of Geophysical Research,110, D05108. https://doi.org/10.1029/2004JD004721

Chang, W., Stein, M. L., Wang, J., Kotamarthi, V. R., & Moyer, E. J. (2016). Changes in spatiotemporal precipitation patterns in changing climate conditions. Journal of Climate, 29, 8355–8376. https://doi.org/10.1175/jcli-d-15-0844.1

Collins, M. J. (2009), Evidence of changing flood risk in New England since the late 20th century, J. Am. Water Resour. Assoc.,42(2), 279–290. https://doi.org/10.1111/j.1752-1688.2008.00277.x

Collins, E. L., Sanchez, G. M., Terando, A., Stillwell, C. C., Mitasova, H., Sebastian, A., & Meentemeyer, R. K. (2022). Predicting flood damage probability across the conterminous United States. *Environmental Research Letters*, *17*(3), 034006. https://doi.org/10.1088/1748-9326/ac4f0f

Condon, L. E., Atchley, A. L., & Maxwell, R. M. (2020). Evapotranspiration depletes groundwater under warming over the contiguous United States. Nature Communications, 11(1), 873. https://doi.org/10.1038/s41467-020-14688-0

Dai, A. (2012). Increasing drought under global warming in observations and models. Nature Climate Change, 3(1), 52–58. https://doi.org/10.1038/nclimate1633

Demaria, E. M. C., Palmer, R. N., & Roundy, J. K. (2016a). Regional climate change projections of streamflow characteristics in the northeast and Midwest U.S. Journal of Hydrology: Regional Studies,5, 309–323. https://doi.org/10.1016/j.ejrh.2015.11.007

Demaria, E. M. C., Roundy, J. K., Wi, S., & Palmer, R. N. (2016b). The effects of climate change on seasonal snowpack and the hydrology of the northeastern and upper Midwest United States. Journal of Climate,29(18), 6527–6541. https://doi.org/10.1175/JCLI-D-15-0632.1

Dhakal N, Palmer RN. Changing River Flood Timing in the Northeastern and Upper Midwest United States: Weakening of Seasonality over Time? *Water*. 2020; 12(7):1951. https://doi.org/10.3390/w12071951

Donner, L. J., Wyman, B. L., Hemler, R. S., Horowitz, L. W., Ming, Y., Zhao, M., et al. (2011). The dynamical core, physical parameterizations, and basic simulation characteristics of the atmospheric component AM3 of the GFDL global coupled model CM3. Journal of Climate, 24(13), 3484–3519. https://doi.org/10.1175/2011jcli3955.1

Fyfe, J. C., Derksen, C., Mudryk, L., Flato, G. M., Santer, B. D., Swart, N. C., et al. (2017). Large near-term projected snowpack loss over the western United States. Nature Communications,8, 14996. https://doi.org/10.1038/ncomms14996

Garner, A. J., Kopp, R. E., & Horton, B. P. (2021). Evolving tropical cyclone tracks in the North Atlantic in a warming climate. Earth's Future, 9, e2021EF002326. https://doi.org/10.1029/2021EF002326

Gent, P. R., Danabasoglu, G., Donner, L. J., Holland, M. M., Hunke, E. C., Jayne, S. R., et al. (2011). The community climate system model version 4. Journal of Climate, 24(19), 4973–4991. https://doi.org/10.1175/2011JCLI4083.1

Gochis, D. J., and F. Chen (2003). Hydrological enhancements to the community Noah land surface model. NCAR Scientific Tech. Rep. TN-4541STR, 77 pp., https://doi.org/10.5065/D60P0X00

Gochis, D.J., M. Barlage, R. Cabell, M. Casali, A. Dugger, K. FitzGerald, M. McAllister, J. McCreight, A. RafieeiNasab, L. Read, K. Sampson, D. Yates, Y. Zhang (2020). The WRF-Hydro® modeling system technical description, (Version 5.1.1). NCAR Technical Note. 107 pages. Available online at: https://ral.ucar.edu/sites/default/files/public/WRFHydroV511TechnicalDescription.pdf.

Gori A, Lin N, Xi D, Emanuel K. (2022). Tropical cyclone climatology change greatly exacerbates US extreme rainfall-surge hazard. Nat Clim Chang. 12:171–178. https://doi.org/10.1038/s41558-021-01272-7

Grogan, D. S., Burakowski, E. A., & Contosta, A. R. (2020). Snowmelt control on spring hydrology declines as the vernal window lengthens. Environmental Research Letters,15(11), 1–9. https://doi.org/10.1088/1748-9326/abbd00

Guilbert, J., Betts, A. K., Rizzo, D. M., Beckage, B., & Bomblies, A. (2015). Characterization of increased persistence and intensity of precipitation in the northeastern United States. Geophysical Research Letters,42, 1888–1893. https://doi.org/10.1002/2015GL063124

Groisman, P. Y., R. W. Knight, D. R. Easterling, T. R. Karl, G. C. Hegerl,V. N. Razuvaev, and N. Vyacheslav (2005).Trends in intense precipitation in the climate record, J. Clim.,18, 1326–1350. https://doi.org/10.1175/JCLI3339.1

Hayhoe, K., Wake, C.P., Huntington, T.G. et al. (2007). Past and future changes in climate and hydrological indicators in the US Northeast. Clim Dyn 28**,** 381–407. https://doi.org/10.1007/s00382-006-0187-8

Hodgkins, G.A.; Dudley, R.W.; Huntington, T.G. Changes in the timing of high river flows in New England over the 20th Century. J. Hydrol. **2003**, 278, 244–252. https://doi.org/10.1016/S0022-1694(03)00155-0

Horton, R., Yohe, G., Easterling, W., Kates, R.; Ruth, M., Sussman, E., Whelchel, A., Wolfe, D., Lipschultz, F. (2014) Chapter 16: Northeast. In Climate Change Impacts in the United States: The Third National Climate Assessment; Melillo, J.M., Richmond, T.T.C., Yohe, G.W., Eds.; U.S. Global Change Research Program: Washington, DC, USA.

Huntington, T. G., A. D. Richardson, K. J. McGuire, and K. Hayhoe (2009), Climate and hydrological changes in the northeastern United States: Recent trends and implications for forested and aquatic ecosys-tems, Can. J. For. Res.,39, 199–212. https://doi.org/10.1139/X08-116

Hu, X., Sejas, S.A., Cai, M. *et al.* (2019). Decadal evolution of the surface energy budget during the fast warming and global warming hiatus periods in the ERA-interim. Clim Dyn 52**,** 2005–2016. https://doi.org/10.1007/s00382-018-4232-1

Jones, C. D., et al. (2011), The HadGEM2-ES implementation ofCMIP5 centennial simulations, Geosci. Model Dev.,4(3), 543–570. https://doi.org/10.5194/gmd-4-543-2011

Kam, J.; Sheffield, J. Changes in the low flow regime over the eastern United States (1962–2011): Variability, trends, and attributions. Clim. Chang. **2016**, 135, 639–653. https://doi.org/10.1007/s10584-015-1574-0

Karmalkar, A. V., & Bradley, R. S. (2017). Consequences of global warming of 1.5°C and 2°C for regional temperature and precipitation changes in the contiguous United States. PLoS One,12, e0168697. https://doi.org/10.1371/journal.pone.0168697

Konapala, G., Mishra, A. K., Wada, Y., & Mann, M. E. (2020). Climate change will affect global water availability through compounding changes in seasonal precipitation and evaporation. Nature Communications, 11(1), 3044. https://doi.org/10.1038/s41467-020-16757-w

Kotamarthi, R., Hayhoe, K., Mearns, L., Wuebbles, D., Jacobs, J., & Jurado, J. (2021). Dynamical Downscaling. In *Downscaling Techniques for High-Resolution Climate Projections: From Global Change to Local Impacts* (pp. 64-81). Cambridge: Cambridge University Press. https://doi.org/10.1017/9781108601269.005

Kulp, S. A., & Strauss, B. H. (2019). New elevation data triple estimates of global vulnerability to sea-level rise and coastal flooding. Nature Communications, 10(1), 4844. https://doi.org/10.1038/s41467-019-12808-z

Leta, O. T., El-Kadi, A. I., Dulai, H., and Ghazal, K. A. (2016). Assessment of climate change impacts on water balance components of Heeia watershed in Hawaii, J. Hydrol.-Regional Studies 8, 182–197. https://doi.org/10.1016/j.ejrh.2016.09.006

Marshall, E., and T. Randhir (2008). Effect of climate change on watershed system: A regional analysis, Clim. Change,89, 263–280. https://doi.org/10.1007/s10584-007-9389-2

Melillo, J. M., T. C. Richmond, and G. W. Yohe (2014), Climate change impacts in the United States: The third National Climate Assessment, U.S. Global Change Research Program, Global

Change Research Program, Washington, D. C. https://www.nrc.gov/docs/ML1412/ML14129A233.pdf
Naz, B. S., Kao, S. C., Ashfaq, M., Rastogi, D., Mei, R., and Bowling, L. C. (2016). "Regional hydrologic response to climate change in the conterminous United States using high-resolution hydroclimate simulations." Global and Planetary Change, 143, 100–117. https://doi.org/10.1016/j.gloplacha.2016.06.003
Niu, G.-Y., Yang, Z.-L., Mitchell, K. E., Chen, F., Ek, M. B., Barlage, M., et al. (2011). The Community Noah Land Surface Model with Multi-Parameterization Options (NOAH-MP): 1. Model description and evaluation with local-scale measurements. Journal of Geophysical Research, 116, D12109. https://doi.org/10.1029/2010JD015139
Pachauri, R. K., Allen, M. R., Barros, V. R., Broome, J., Cramer, W., Christ, R., Church, J. A., Clarke, L., Dahe, Q. D., Dasqupta, P., Dubash, N. K., Edenhofer, O., Elgizouli, I., Field, C. B., Forster, P., Friedlingstein, P., Fuglestvedt, J., Gomez-Echeverri, L., Hallegatte, S., ... van Ypersele, J-P. (2014). Climate change 2014 synthesis report. contribution of working groups I, II, and III to the fifth assessment report of the Intergovernmental Panel on Climate Change. IPCC. http://www.mendeley.com/research/climate-change-2014-synthesis-report-contribution-working-groups-i-ii-iii-fifth-assessment-report-in-20
Pal, S., Chang, H.-I., Castro, C. L., & Dominguez, F. (2019). Credibility of convection-permitting modeling to improve seasonal precipitation forecasting in the southwestern United States. Frontiers in Earth Science,7, 11. https://doi.org/10.3389/feart.2019.00011
Pal, S., Dominguez, F., Dillon, M. E., Alvarez, J., Garcia, C. M., Nesbitt, S. W., & Gochis, D. (2021a). Hydrometeorological observations and modeling of an extreme rainfall event using WRF and WRF-Hydro during the RELAMPAGO field campaign in Argentina, Journal of Hydrometeorology, 22(2), 331–351. https://doi.org/10.1175/JHM-D-20-0133.1
Pal, S., Dominguez, F., Bollatti, P., Oncley, S. P., Yang, Y., Alvarez, J., & Garcia, C. M. (2021b). Investigating the effects of land use change on subsurface, surface, and atmospheric branches of the hydrologic cycle in central Argentina. Water Resources Research, 57, e2021WR029704. https://doi.org/10.1029/2021WR029704
Parr, D., and G. Wang (2015a), Hydrological changes in the U.S. Northeast using the Connecticut River Basin as a case study: Part 1. Modeling and analysis of the past, Global Planet. Change,122, 208–222. https://doi.org/10.1016/j.gloplacha.2014.08.009
Parr, D., Wang, G., & Ahmed, K. F. (2015b). Hydrological changes in the U.S. northeast using the Connecticut River basin as a case study: Part 2. Projections of the future. Global and Planetary Change,133, 167–175. https://doi.org/10.1016/j.gloplacha.2015.08.011
Pendergrass, A. G., Knutti, R., Lehner, F., Deser, C., & Sanderson, B. M. (2017). Precipitation variability increases in a warmer climate. Scientific Reports,7(1), 1–9. https://doi.org/10.1038/s41598-017-17966-y
Pringle, W. J., Wang, J., Roberts, K. J., & Kotamarthi, V. R. (2021). Projected changes to cool-season storm tides in the 21st century along the northeastern United States coast. Earth's Future, 9, e2020EF001940. https://doi.org/10.1029/2020EF001940
Quansah JE, Naliaka AB, Fall S, Ankumah R, Afandi GE. (2021) Assessing Future Impacts of Climate Change on Streamflow within the Alabama River Basin. Climate, 9(4):55. https://doi.org/10.3390/cli9040055
Schwalm, C. R., Glendon, S., & Duffy, P. B. (2020). RCP8.5 tracks cumulative CO_2 emissions. Proceedings of the National Academy of Sciences of the United States of America,117, 19,656–19,657. https://doi.org/10.1073/PNAS.2007117117

Seaber, PR, Kapinos FP, Knapp GL (1987) Hydrologic unit maps. U. S. Geological Survey Water-Supply Paper 2294. U.S. Geological Survey, Denver, Colorado. https://pubs.usgs.gov/wsp/wsp2294/pdf/wsp_2294_a.pdf

Seneviratne, S. I., et al. (2012). Changes in climate extremes and their impacts on the natural physical environment, in Managing the Risks of Extreme Events and Disasters to Advance Climate Change Adaptation, edited by C.B. Fieldetal. A Special Report of Working Groups I and II of the Intergovernmental Panel on Climate Change (IPCC) , pp. 109–230 , Cambridge University Press, U. K. https://doi.org/10.7916/d8-6nbt-s431

Shaw, S. B., A. A. Royem, and S. J. Riha (2011), The relationship between extreme hourly precipitation and surface temperature in different hydroclimatic regions of the United States, J. Hydrometeorol.,12(2),319–325. https://doi.org/10.1175/2011JHM1364.1

Sherwood, S. C., Bony, S., & Dufresne, J. L. (2014). Spread in model climate sensitivity traced to atmospheric convective mixing. Nature, 505(7481), 37–42. https://doi.org/10.1038/nature12829

Siddique, R., A. Karmalkar, S. Fengyun, and R.N. Palmer. (2020). Hydrological Extremes across the Commonwealth of Massachusetts. Journal of Hydrology: Regional Studies,32:100733. https://doi.org/10.1016/j.ejrh.2020.100733

Siddique R., A. Mejia, N. Mizukami, R. Palmer (2021). Impacts of global warming of 1.5, 2.0 and 3.0 °C on hydrologic regimes in the Northeastern U.S. Climate, 9 (1), p. 9. https://doi.org/10.3390/cli9010009

Skamarock, W. C., Klemp, J. B., Dudhia, J., Gill, D. O., Barker, D., Duda, M. G., … Powers, J. G. (2008). A Description of the Advanced Research WRF Version 3 (No. NCAR/TN-475+STR). University Corporation for Atmospheric Research. http://dx.doi.org/10.5065/D68S4MVH

Somos-Valenzuela, M.A., and R.N. Palmer. (2018) Use of WRF-Hydro over the Northeast of the US to Estimate Water Budget Tendencies in Small Watersheds. Water 10 (12): 1709. https://doi.org/10.3390/w10121709.

Sunde, M.G., H.S. He, J.A. Hubbart, and M.A. Urban. (2017). "Inte-grating Downscaled CMIP5 Sata with a Physically Based Hydrologic Model to Estimate Potential Climate Change Impacts on Streamflow Processes in a Mixed-Use Watershed." Hydrological Processes,31 (9): 1790–803. https://doi.org/10.1002/hyp.11150.

Tebaldi, C., K. Hayhoe, J. M. Arblaster, and G. A. Meehl (2006). Going to the extremes, Clim.Change,79(3–4), 185–211. https://doi.org/10.1007/s10584-006-9051-4

Trenberth, K. E. (1999). Conceptual framework for changes of extremes of the hydrological cycle with climate change, Clim. Change,42(1),327–339. https://doi.org/10.1023/A:1005488920935

Villarini, G. (2016), On the Seasonality of Flooding Across the Continental United States, Adv. Water Resour.,87,80–91. https://doi.org/10.1016/j.advwatres.2015.11.009

Walsh, J., and Coauthors (2014). Our changing climate. Climate change impacts in the United States: The Third National Climate Assessment, J. M. Melillo, T. C. Richmond, and G. W. Yohe, Eds., U.S. Global Change Research Program Rep., 19–67, https://doi.org/10.7930/J0KW5CXT.

Wang, J., & Kotamarthi, V. R. (2015). High-resolution dynamically downscaled projections of precipitation in the mid and late 21st century over North America. Earth's Future, 3, 268–288. https://doi.org/10.1002/2015EF000304

Wang, J., Wang, C., Rao, V., Orr, A., Yan, E., & Kotamarthi, R. (2019). A parallel workflow implementation for PEST version 13.6 in high-performance computing for WRF-hydro version 5.0: A case study over the midwestern United States. Geoscientific Model Development,12(8), 3523–3539. https://doi.org/10.5194/gmd-12-3523-2019

Wobus C, Porter J, Lorie M, Martinich J, Bash R. Climate change, riverine flood risk and adaptation for the conterminous United States. Environ Res Lett. 2021 Aug 31;16(9) https://dx.doi.org/10.1088%2F1748-9326%2Fac1bd7

Wuebbles D. J, D.W. Fahey, K.A. Hibbard, J.R. Arnold, B. DeAngelo, S. Doherty, D.R. Easterling, J. Edmonds, T. Edmonds, T. Hall (2017). Climate Science Special Report: Fourth National Climate Assessment (NCA4), Volume I

Xia, Y., Mitchell, K., Ek, M., Sheffield, J., Cosgrove, B., Wood, E., Luo, L., Alonge, C., Wei, H., Meng, J., Livneh, B., Lettenmaier, D., Koren, V., Duan, Q., Mo, K., Fan, Y., and Mocko, D. (2012). Continental-scale water and energy flux analysis and validation for the North American Land Data Assimilation System project phase 2 (NLDAS-2), 1: Intercomparison and application of model products, J. Geophys. Res., 117, D03109, https://doi.org/10.1029/2011JD016048

Yin, J., Schlesinger, M. E., & Stouffer, R. J. (2009). Model projections of rapid sea-level rise on the northeast coast of the United States. Nature Geoscience,2, 262–266. https://doi.org/10.1038/ngeo462

Zobel, Z., Wang, J., Wuebbles, D. J., & Kotamarthi, V. R. (2017). High-resolution dynamical downscaling ensemble projections of future extreme temperature distributions for the United States. Earth's Future,5, 1234–1251. https://doi.org/10.1002/2017EF000642

Zobel, Z., Wang, J., Wuebbles, D. J., & Kotamarthi, V. R. (2018a). Evaluations of high-resolution dynamically downscaled ensembles over the contiguous United States. Climate Dynamics, 50(3–4), 863–884. https://doi.org/10.1007/s00382-017-3645-6

Zobel, Z., Wang, J., Wuebbles, D. J., &Kotamarthi, V. R. (2018b). Analyses for high-resolution projections through the end of the 21st century for precipitation extremes over the United States. Earth's Future,6, 1471–1490. https://doi.org/10.1029/2018EF000956